Nanocluster aerosol emissions of a 3D printer

Mikko Poikkimäki,*,† Ville Koljonen,† Niko Leskinen,† Mikko Närhi,‡ Oskari Kangasniemi,† Oskari Kausiala,† and Miikka Dal Maso†

†*Aerosol Physics Laboratory, Physics Unit, Tampere University, FI-33720, Tampere, Finland*

‡*Photonics Laboratory, Physics Unit, Tampere University, FI-33720, Tampere, Finland*

E-mail: mikko.poikkimaki@tuni.fi

Abstract

Many studies exist characterizing the aerosol emissions from fuse filament fabrication three-dimensional (3D) printers. However, nanocluster aerosol (NCA) particles are rarely studied meaning size range under 3 nm. The purpose of this study was to characterize the NCA emissions and the contribution of NCA to the total number emissions from a 3D printer. We used a particle size magnifier (PSM) and a scanning mobility particle sizer (SMPS) to measure the time evolution of particle size distribution, which was used to calculate the average NCA emission rates during a printer operation in a chamber. The NCA emission rates ranged from $1.4{\cdot}10^6$ to $7.3{\cdot}10^9$ s^{-1} depending on the applied combination of filament material and nozzle temperature, showing increasing emission with increasing temperature. The NCA emissions constitute from 9 up to 48 percent of the total emissions, i.e., almost half of the particle emissions may have been previously neglected. Therefore, it is essential to include the low NCA size range in, e.g., future 3D printer testing protocols, emission measurements standards and risk management measures.

Introduction

Three-dimensional (3D) printers enable easy and inexpensive fabrication of items with complex shapes, which is an important reason for their increasing utilization. They are widely operated in many indoor environments, such as homes, schools and offices, due to their low price and good availability. The popularity of 3D printers has especially grown in school classrooms and university libraries, where they are used for educational purposes.[1] On the other hand, the wide application of 3D printing has given rise to health concerns, related to the fumes emitted during the printing process,[2] and the possible user exposure to the fumes in low-ventilated environments.

Recent studies have shown that exposure to 3D printing can cause respiratory symptoms[3] and increase in exhaled nitric oxide,[4] which is a sign of asthma, in humans. Others also have shown cardiovascular symptoms in animals after inhalation[5] and negative impact on animal embryo development.[6] Moreover, nano-sized particles emitted in aerosol form[7] from 3D printers can induce not only cell death and oxidative stress in human airway epithelial cells[8] but also inflammatory responses in mice.[9] The aerosol nanoparticles can also potentially enter the blood circulation by penetrating into the alveolar region of the lung upon inhalation.[10] The nanoparticles can then reach sensitive areas, such as the bone marrow, spleen or heart, posing health risks.[11] Therefore, a detailed characterization of the emissions from 3D printers is important for risk assessments.

Numerous studies have shown that 3D printers emit a large amount of aerosol nanoparticles with diameters starting from 4 nm.[12–32] Most of the studies have concentrated on printers that employ the fused deposition modeling (FDM) or so-called fuse filament fabrication (FFF) method, since these printers are readily available for many consumers. A common observation for the FFF studies is that the emissions depend on the printing conditions, such as printing temperatures, and on the used filament materials. The studied materials include polymer thermoplastics, such as acrylonitrile-butadiene-styrene (ABS), polylactic acid (PLA) and PLA varieties containing additives, such as wood and metals. However, the

market has expanded to offer large variety of other materials as well, which remain unstudied.

In the light of aerosol emissions, an important printing condition is the nozzle temperature, since at high enough temperatures the material is heated enough and can vaporize causing airborne emissions. The effect of nozzle temperature as well as filament material have been previously studied, but the results vary between the studies. For example, Azimi et al. found a weak to no correlation between the particle emissions and the nozzle temperature,[15] whereas Deng et al., Zhang et al., Mendes et al. and Stabile et al. found a positive correlation.[20,24,33,34] Thus, there is a need to further study the combined effect of filament material and the nozzle temperature to find stronger evidence on the actual reason.

Despite the numerous studies on 3D printer emissions,[35] data on particles less than 3 nm in diameter is still limited. Rönkkö et al. introduced the term nanocluster aerosol (NCA) to refer to these particles in the size-range of 1.3 - 3 nm and that term is adapted here.[36] The study on NCA is especially important, since NCA might have different health effects compared to larger sized particles. This difference results from effective deposition due to diffusion in the head air ways, from where, particles potentially migrate to brain[37] causing neural effects.[38] However, the effects of NCA are mostly unknown. Therefore, it is of importance to study the small cluster sized particles and track their growth to better understand the printing process and the potential health impacts.

Ahonen et al. published measurements of 1-2 nm sized particles during manufacturing processes of electronics in a clean room. They found notable nanocluster aerosol concentrations,[39] but the results can not be directly applied to 3D printing. Moreover, NCA has been found to constitute a significant fraction of the traffic-emitted aerosol[36,40,41]as well as urban air aerosol concentrations.[42,43] As a matter of fact, nanoclusters play a key role also in the natural atmospheric aerosol formation.[44,45] Thus, to understand the formation mechanism and origin of the aerosol emissions from 3D printing, it is crucial to study the NCA as the clusters can act as seeds for particle growth eventually determining the particle properties.[46,47]

Mendes et al. were the first ones to study particle emissions from a FFF 3D printer in the low NCA size range.[34] They found a high number of particles in this size range during all the tested printing periods. However, they reported the total particle number concentration of the NCA, and thus, the size resolved particle emission rates still remain to be measured for the NCA. Emission rate is a critical parameter determining the concentration level in the vicinity of the source, and by measuring it, the environmental conditions, such as air exchange rate, are normalized for. Therefore, the emission rate is more representative of the 3D printer as a source, and measured emission rates can be used to predict the concentrations, and ultimately the exposure, near the printer.

The objective of this study is to characterize the NCA and fine particle emissions to detect the effects of the nozzle temperature and filament material as well as the contribution of NCA to the total emissions. This was done by measuring and calculating the emission rates of NCA and fine particles in the 1 nm to 1 μm size range during FFF 3D printing process. The study applies five different filament materials and four different nozzle temperatures to determine the combined effect of the temperature and material. The obtained particle emission rates are compared to those obtained in previous studies to create a stronger link between the emissions and the printing conditions. Finally, we also show a simple example of an application of the emission rate in modelling the nanoparticle exposure in the vicinity of the 3D printer.

Materials and methods

3D printer and FFF method. The printer employed in this study is a commercial 3D printer called Ultimaker 2 (Ultimaker B.V., Geldermalsen, The Netherlands). The printer utilizes the fuse filament fabrication (FFF) or material extrusion method. In the FFF method, a filament material is fed to a narrow heated nozzle with a constant speed. The material is melted at the nozzle and extruded through it onto a heated bed. During the

extrusion, the nozzle is moving in a frame in three dimensions by a predetermined program to form the desired object layer by layer. In this study, the printed object was a frog with maximum dimensions of approximately 5.5 x 4.6 x 2.5 cm^3 and the printing took in average 36 minutes, see SI I for printer details.

Filament materials and nozzle temperatures. The frog object was printed by using five different filament materials. The first employed material was acrylonitrile butadiene styrene (ABS, red by Ultimaker), which is among the most common materials in consumer use. Another commonly used filament is polylactic acid (PLA), for which three different varieties were used: one without additives (Ultimate Blue by Ultimaker), one with wood additive (woodFill by colorFabb) and one with copper additive (copperFill by colorFabb). Finally, a polyester filament (nGEN by colorFabb) was used. The filament materials were printed using varying nozzle temperatures of 210, 220, 240 and 250 °C. The materials were tested in the temperatures recommended by the manufacturer as well as above of those temperatures. The bed temperature was kept constant at 70, 80 or 90 °C, depending on the manufacturer recommendation for each material, and thus, is not in the focus in this study.

A total of 10 different material-temperature combinations were studied. The same combination was repeated two to three times yielding a total of 22 successful prints, see Table 1. Due to this small sample size (n = 2 or 3), we were not able to perform statistical comparisons between the material-temperature combinations, thus only descriptive comparisons were made. In addition, the experiments included a number of failed prints, resulting from incompatibilities of the material-temperature combinations, see SI II. The focus of this paper is in the successful prints; emission characteristics of failed prints will be discussed briefly as they still represent a potential emission scenario in normal consumer operation.

Aerosol sampling. The measurements were performed in an aerosol laboratory at Tampere University between 24th and 31st of March 2017. For the emission rate measurements, the 3D printer was placed in a contained chamber with the volume of 300.0 ± 5.3 Liters to avoid influence from the laboratory air, see Fig. 1 . The chamber was flushed using HEPA

filtered air with a mass flow of 100 ± 1 lpm (flow controller by Alicat Scientific Inc., USA) providing constant dilution and mixing to the chamber. Due to this high air exchange rate of 20 h^{-1}, the air in the chamber is expected to be well mixed. The dilution flow was directed away from the printer nozzle to the back wall of the chamber to avoid direct influence to the nozzle and, hence, the printing process itself. The aerosol was sampled directly from the chamber and directed to the aerosol instrumentation.

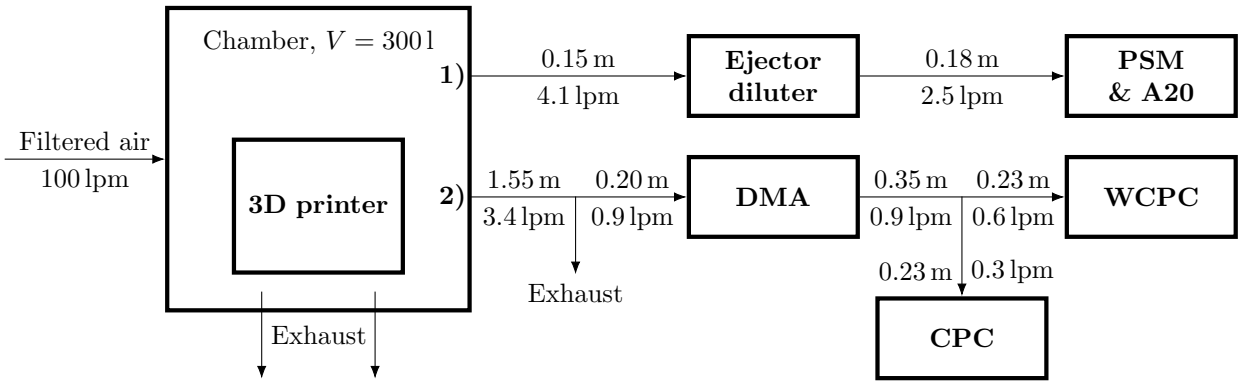

Figure 1: A schematic diagram of the measurement setup.

We used two sampling lines, one for concentration and another for size distribution measurements. The first sampling line, which was used to study the NCA size range, was kept as short as possible to minimize particle losses since the diffusion losses are expected to be high for the smallest particles. The line was also made of conducting material to avoid losses of charged particles. Moreover, an ejector diluter was needed due to high NCA concentrations. A second sampling line was used for size distribution measurements; as the differential mobility analyzer (DMA) itself causes dilution, the aerosol would have been too diluted for reliable particle size distribution measurement otherwise.

The first sampling line led the aerosol from the chamber to nCNC A11 instrumentation (Airmodus Ltd, Finland) consisting of a particle size magnifier (PSM A10) and a condensation particle counter (CPC A20) measuring total particle number concentration (1.4 - 1000 nm) and number size distribution (1.4 - 4.3 nm). The PSM was run in the step mode with a time resolution of 30 seconds/step using four saturator flows of 1.2, 0.3,

0.15 and 0.1 lpm. These saturator flows correspond to particle activation sizes of 1.4 ± 0.1, 1.75 ± 0.1, 3.15 ± 0.3 and 4.3 ± 0.3 nm according to the calibration data by the manufacturer, see SI IV. The calibration was done for nickel chromium particles, whereas the particle composition of 3D printer emissions is probably different. This might alter the particle activation in the PSM, and hence, the diameter estimation by up to 1 nm based on previous experience.[48]

The sample to PSM was taken through an ejector diluter (Dekati Ltd, Finland), for which the dilution ratio (DR) was calculated by comparing total number concentration with and without the diluter resulting in an average DR of 12.2 ± 0.9. (taking into account the dilution and particle losses in the diluter). Note that the DR estimation was only possible for total number concentrations, while the particle losses are, in reality, higher in the NCA size range and lower for larger particle sizes. This probably causes an underestimation to the NCA concentration. In addition to the diffusion losses, the concentration data was corrected for the maximal PSM efficiency of 77.3 ± 1.5 percent according to the calibration data (SI IV).

The second sampling line fed the aerosol to a custom build scanning mobility particle sizer (SMPS) consisting of a Kr-85 aerosol neutralizer, a differential mobility analyzer (DMA, TSI model 3085, sheath flow 18.0 ± 0.1 lpm), a butanol condensation particle counter (CPC, TSI model 3775) and a water condensation particle counter (WCPC, TSI model 3786). The SMPS was used to measure the particle number size distribution in the range of 4.0 - 57.3 nm with a resolution of 180 seconds. The concentration values were corrected for diffusion losses in the sampling lines (Tygon E-3603) according to Kulkarni et al.[49] ($\eta = \exp -\xi \cdot Sh$) by using the sample flow rates (Gilibrator flow meter, Sensidyne LP, USA) and line lengths presented in Fig. 1.

The emission characterization in the chamber. The behaviour of the aerosol population in the chamber can be described as follows. The measured number concentration $N(t)$ in the chamber changes over time t due to the emissions from the 3D printer and the particle

losses in the chamber. The change of the particle number in time follows the equation:[34]

$$\frac{\mathrm{d}N}{\mathrm{d}t} = Q(t) - \left(\beta + \gamma - \sum_i K_i N_i\right) N(t), \tag{1}$$

where $Q(t)$ is the emission rate ($\mathrm{cm^{-3}s^{-1}}$), β is deposition rate to the chamber walls ($\mathrm{s^{-1}}$), γ is dilution coefficient due to the dilution flow to the chamber ($\mathrm{s^{-1}}$) and $\sum_i K_i N_i$ is the coagulation sink ($\mathrm{s^{-1}}$) for the aerosol population consisting of i different size-ranges. The change in the concentration ($\mathrm{d}N/\mathrm{d}t$) is calculated from the measurement data for each time step. The dilution coefficient γ can be calculated from the flow of filtered air to the chamber ($5.6 \pm 0.2 \cdot 10^{-3}$ $\mathrm{s^{-1}}$), whereas the coagulation sink is calculated from the size distribution data (10^{-6} to $5.7 \cdot 10^{-3}$ $\mathrm{s^{-1}}$). However, the deposition term is not directly known and needs to be determined from the data.

By assuming coagulation sink to be only weakly time-dependent and the source term $Q(t)$ to be zero, the equation 1 can be simplified to

$$N(t) = N_0\, e^{-t(\beta+\gamma-\sum_i K_i N_i)}, \tag{2}$$

which is an exponential decay in the concentration. This kind of situation appears when the printing process has finished and we can assume that the particle source disappears. Therefore, an exponential fit can be made to the measured concentration data to calculate the loss terms. Since the other loss terms are already known, the deposition rate β can be estimated from Eq. 2. The rate was calculated using data fits from several print process endings (n = 19) resulting in an average deposition rate of $9.6 \pm 1.5 \cdot 10^{-3}$ $\mathrm{s^{-1}}$. In reality, the deposition rate is size dependent, and therefore, the NCA emissions can be underestimated as the NCA deposition in the chamber is probably higher than the average used in this study. Finally, we calculated the size resolved and total emission rates Q from Eq. 1.

Indoor user exposure modeling. We used the NCA and total emission rates to model two exposure scenarios. For the first scenario, we assumed a laboratory room with dimensions

of 9 m x 6 m x 3 m and ventilation rate of 18 h^{-1}, similar as in Ref. 50, whereas the other scenario was a regular home room with dimensions of 4 m x 4 m x 2.5 m and ventilation rate of 0.5 h^{-1}. Both cases had the same turbulent diffusion coefficient of 0.002 m^2s^{-1} to allow better comparison. The model used here is an computational implementation of the indoor diffusion model presented by Drivas et al.[51] The particle number concentration in the room location (x, y, z) results from an instantaneous source q (number of particles) and can be calculated as a function of time t (s) from the emission start

$$c_{inst}(x, y, z, t) = \frac{q}{(4\pi Kt)^{3/2}} \exp(-at + \frac{w_d A}{V} t) R_x R_y R_z, \tag{3}$$

where a (s^{-1}) is the ventilation rate, w_d (m/s) deposition rate, set to zero for simplicity, A (m^2) deposition surface area, V (m^3) room volume, K (m^2/s) effective indoor turbulent diffusion coefficient and R_x, R_y, R_z are the dimensionless wall reflection terms for a rectangular room, see Drivas et al. equations 5, 6 and 7. The equation 3 can be extended to constantly emitting source Q (s^{-1}), such as 3D printer, by integrating over the emission time t_{emis}

$$c_{cont}(x, y, z, t_{emis}) = \int_0^{t_{emis}} \frac{Q}{(4\pi Kt)^{3/2}} \exp(-at + \frac{w_d A}{V} t) R_x R_y R_z dt. \tag{4}$$

A more detailed description with the model source code is found in SI V.

Results and discussion

Concentrations and number size distributions. Figure 2 presents total number concentrations and SMPS size distribution for one example printing process (nGEN at 240°C), while further figures can be found in SI VI. First, the printer bed is heating for a few minutes during which the concentrations stay at background levels. After that, the printer nozzle is heated for 1 to 2 minutes. During which, as the filament material (residual from earlier prints) resides in the nozzle, the material itself can heat up rapidly reaching evaporation

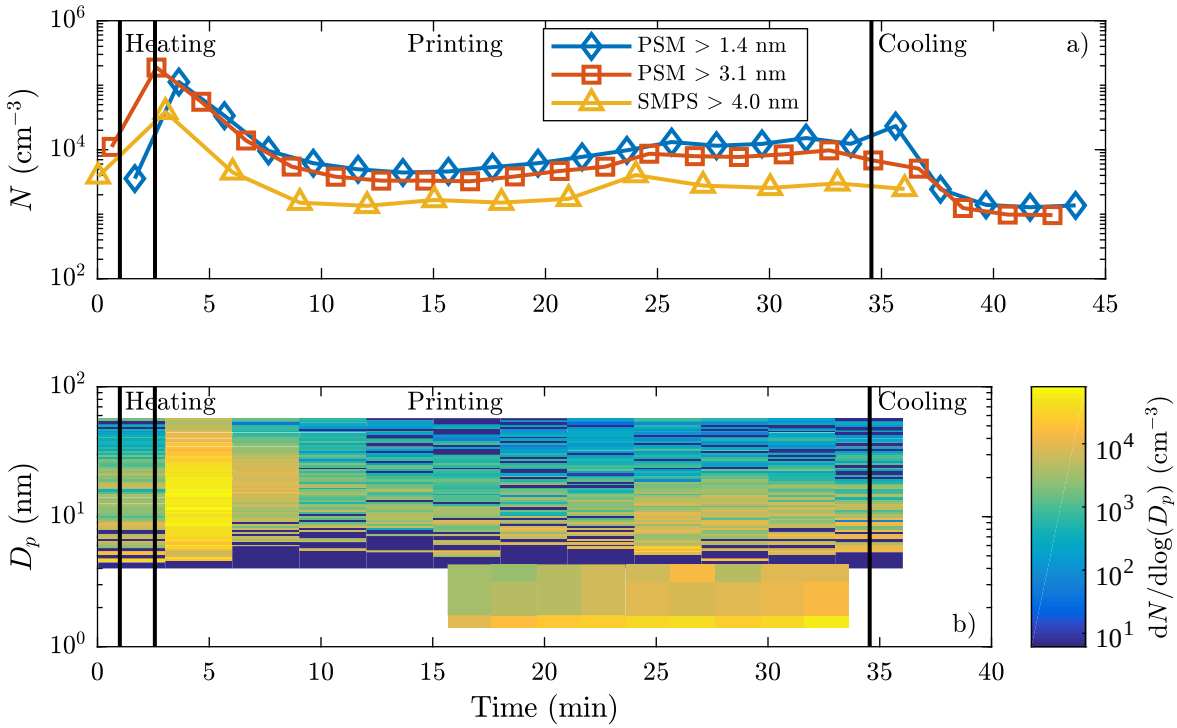

Figure 2: Total particle number concentrations (a) and size distribution (b) in the chamber during a printing process of nGEN filament in temperature of 240 °C (print no. 27). The concentrations are reported for PSM for particles over 1.4 nm and over 3.15 nm as well as for SMPS in size range from 4.0 to 57 nm in diameter. The PSM size distribution (1.4 to 4.3 nm) is presented only for the steady-state situation.

temperature, thus, yielding high particle formation and emission rates. This results in a rapid increase of the number concentrations. The concentrations increase further, at the beginning of the printing process, reaching a peak value. After this initial peak, as the material starts to continuously flow through the nozzle, concentrations decrease immediately reaching a more or less steady-state situation in which there are no rapid concentration changes. This allows an explicit determination of the concentration gradient over time, and, therefore, the further examination as well as the calculation of the emission rate are done only for the steady-state situation.

Figure 3 presents average steady-state number size distributions for the nGEN material printed in three different temperatures. In the temperature of 220 °C, the distribution has one smaller mode in the nanocluster size (1.4 to 1.7 nm) and another larger nucleation

mode approximately at 15 nm. The larger sized particles dominate the distribution with a contribution of 80 percent. Furthermore, the same modes can be seen in the distributions at the temperatures of 240 and 250 °C, but now having one to three orders of magnitude higher total number. The nanocluster mode has a greater amount of particles that, at 250 °C, are slightly larger in size (1.75 to 3.15 nm), and the nucleation mode particle size decreased from 15 nm to less than 10 nm in size. Thus, in general, the higher printing temperature for this material generates larger amount of particles that have smaller size. Additionally, the comparison of SMPS and PSM data in size range over 3.15 nanometers reveals that there might be another mode of particles between 60 nm to 1 µm as the PSM concentration ($N_{>3nm}$) is 1.4 to 3 times higher than that of SMPS.

Even though the concentrations and size distributions provide valuable insight of the emitted particle population characteristics, the number emission of particles emitted cannot be solely estimated by using concentrations due to the particle losses in the chamber. Therefore, the size-resolved emission rates were computed using the method described in the previous section.

Concentrations in malfunction situations. Originally, more combinations were planned for testing, but materials, such as ABS, PLA and PLA with wood and copper additives, caused difficulties in printing, see SI II. These malfunctions situations are expected in the normal use of the printer as correct temperature and other printing conditions are searched to get good enough quality for the printed object. Thus, they present a potential user exposure episode, as the user might be close to the printer while troubleshooting. During the malfunction situations, the number concentrations in the chamber were mainly of similar magnitude or, in some cases, an order of magnitude higher than in normal printing conditions. This suggest a higher emission rate, and therefore, it is expected that the malfunction situations have similar or higher exposure potential to the user as the normal printing situation. By disregarding the malfunction situations, the estimated exposure potential could be biased to be too low as was also discussed in Refs. 34 and 35. However,

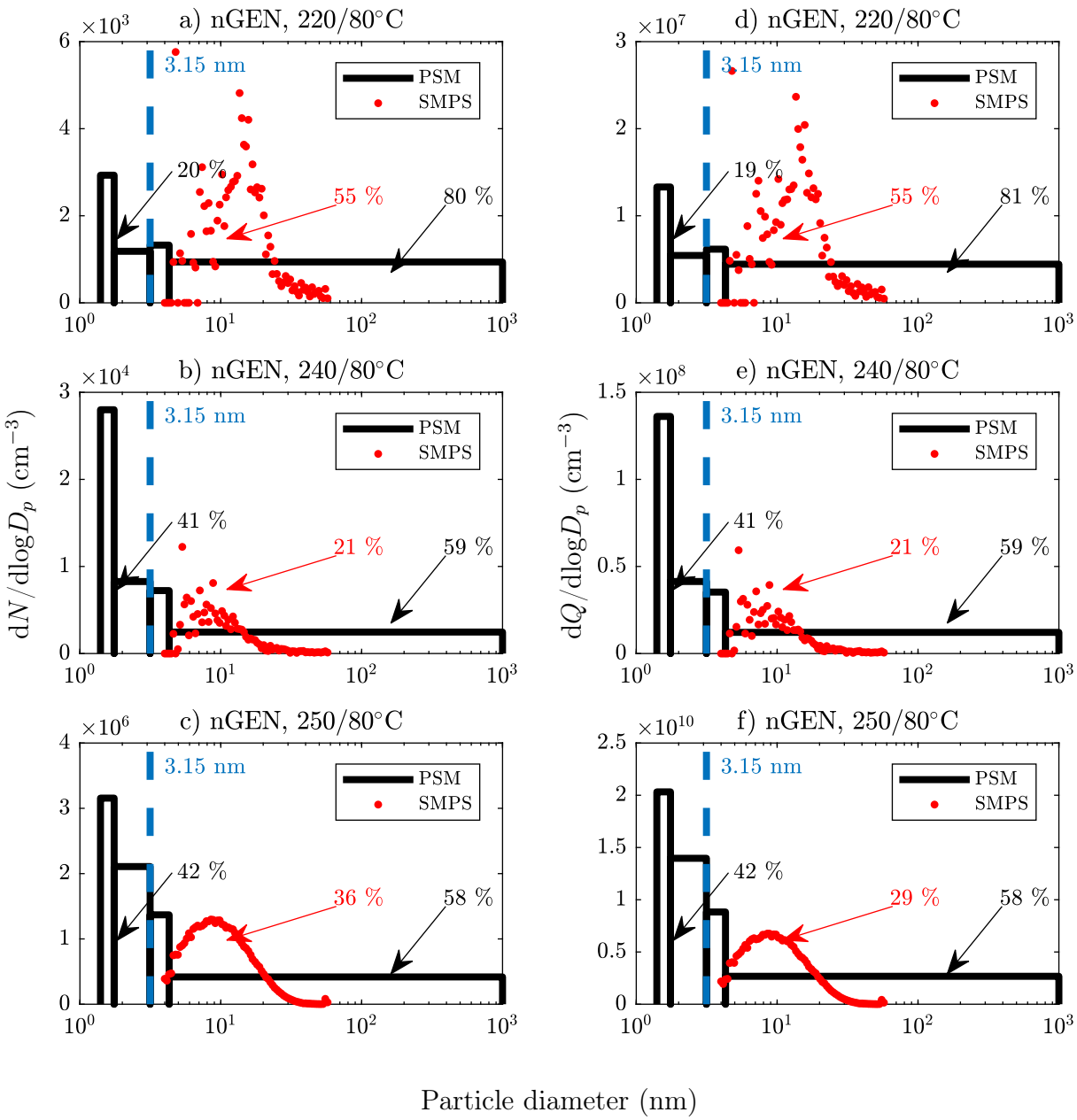

Figure 3: Average steady-state PSM and SMPS particle number size distributions (left panel) and size resolved emission rates (right panel) for nGEN in temperatures of 220, 240 and 250°C for three separate printing events (print no. 27, 30 and 33). The blue vertical line represents the border of the NCA size range. The percentages in each sub-figure represent from left to right the N_{NCA}/N_{tot}, N_{SMPS}/N_{tot} and $N_{>3nm}/N_{tot}$ (left panel), and Q_{NCA}/Q_{tot}, Q_{SMPS}/Q_{tot} and $Q_{>3nm}/Q_{tot}$ (right panel), respectively.

since these malfunction situations resulted mainly from clogged nozzle, and, hence, the frog object could not be fully printed, the main focus of this study is limited to the successful prints for which the full analysis and emission rate calculation was done.

Size resolved emission rates. To provide an estimation of the particle source, emission rates were calculated by equation 1. The right panel of Figure 3 presents the size-dependent emission rate for nGEN material in three different nozzle temperatures. Similarly to the number distributions in the left panel of Fig. 3, the emission rate has one mode at the NCA size range and another mode at the larger sizes. At the temperature of 220°C, the contribution of the NCA to the total emission rate is a notable 13 - 20 percent, while at the higher temperatures of 240 and 250°C, the contribution of NCA increases to no less than 41 - 42 percent. At the same time, when the temperature is increased from 220 to 240°C, the quality of the printed frog object increases significantly, which justifies the higher emission. However, the temperature increase from 240 to 250°C has only a minor effect on the object quality, not justifying the increased emission at 250°C.

NCA emission rates. Figure 4 presents the average steady-state NCA emission rates for size range from 1.4 to 3.15 nm. In total, the emission rates varied from $1.4{\cdot}10^6$ to $7.3{\cdot}10^9$ particles/second depending on the nozzle temperature and the filament material. The differences are further discussed in the following sections.

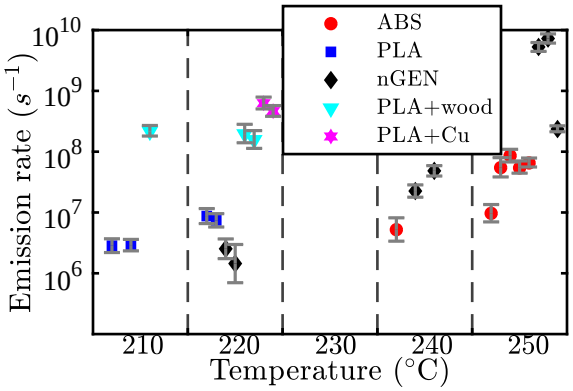

Figure 4: The NCA emission rates (1.4 to 3.15 nm) for different printer filament materials printed using nozzle temperatures of 210, 220, 240 and 250°C. The data points are grouped to distinguish the values obtained for different materials. The error bars mark the limits according to propagation of uncertainty.

Comparison of nozzle temperatures. We observed that the NCA emission rate depends on the nozzle temperature, see Fig. 4. As an overall notion, the NCA emission rates show an increasing trend over the full scale of materials and temperatures. In average, the emission rate increases by almost four orders of magnitude from temperature of 210 to 250°C. However, the comparison of different temperatures for the same material show more evident dependence.

Higher NCA emission rates are observed at higher temperatures for ABS, PLA and nGEN. Firstly, ABS material shows an increase of emissions with increasing temperature if the data point from 240°C is compared to an average value of the five data points from 250°C. As another material, the PLA has a slight increase in the NCA emission rate with increasing temperature, whereas PLA with wood additive exhibits minimal decrease, even though all the values for PLA+wood are within the error limits. The nGEN material was printed in three different temperatures, and the comparison shows the strongest dependence on the temperature. Therefore, in a broader context, the NCA emission rate is clearly dependent on the nozzle temperature. However, as an exception, the PLA with additives showed relatively high emissions compared to materials (ABS and nGEN) that were printed in much higher temperatures. This observation suggests that the emissions are not only dependent on the nozzle temperature, but also the filament material plays an important role.

Comparison of filament materials. The NCA emission rates show differences in the comparison of separate materials printed at the exactly same nozzle temperature, as can be seen in Fig. 4. At the temperature of 210°C, the PLA has lower emission rate compared to the equivalent material with wood additive. Moreover, at the temperature of 220°C, the nGEN has slightly lower emission rate than that of pure PLA and clearly lower than the PLA with wood and copper additives. The PLA with copper additive has the highest NCA emissions at this temperature, even though the PLA with wood exhibits only a minor difference in the inter-comparison. Moreover, the fact that the PLA with additives show high emissions, even at relatively low printing temperatures, calls for characterization of other available filament

materials incorporating additives. At the higher temperatures of 240 and 250°C, the nGEN possesses clearly higher NCA emission rate than that of ABS, and resulted also in the highest NCA and total emission rates obtained in this study. Interestingly, nGEN produced also the lowest observed NCA emission rates.

The differences between filament materials have also been discussed in the previous publications.[35] The PLA has generally shown lower total emission rates than ABS and has been one of the main outcomes of the studies. In contrast, the results of this study suggest that the NCA and total emission rates for PLA at temperatures of 210 and 220°C are similar compared to ABS printed at temperature of 240°C. ABS shows higher emission rates compared to PLA, when printed at higher temperature of 250°C. Therefore, for these two reasons, the differences in emission rates might result from the temperature increase instead of the material itself. Indeed, the results by Kwon et al.,[18] who tested the materials at exact same temperature, suggest that PLA emissions increase significantly when printed at similar temperatures as ABS, however, still showing higher emissions for ABS. However, the material manufacturers do not typically recommend PLA to be printed in such high temperatures as ABS, which is, in like manner, not suggested in the light of these findings. As a limitation, the reader should note that the comparisons of the material-temperature combinations presented here are not based on statistical analysis, and thus, are merely descriptive.

Comparison of different particle sizes: NCA vs total emission rates. The emission rates are divided, in Table 1, to separate particle size ranges, which are denoted as Q_{NCA} with diameter 1.4 - 3.15 nm, Q_{tot} with diameter 1.4 nm - 1 µm and Q_{SMPS} with diameter 4 to 57 nm. In overall, for all different material-temperature combinations tested in the study, the fraction of NCA of total emissions (Q_{NCA}/Q_{tot}) ranged from low 9.3 percent to high 48.0 percent. PLA with wood additive had the lowest NCA fraction (9.3 to 14.5 %) and the highest geometric mean particle count diameter (GMD_{SMPS}, 22 to 24 nm, calculated from SMPS distribution) found in this study, which both suggest that it emits mostly larger particles. PLA with copper additive and ABS have medium NCA fractions from 21.6 to

22.5 % and 16.4 to 30.5 %, respectively. For the latter, the higher temperature increases the total particle count emission and GMD_{SMPS}. Interestingly, the fraction of NCA also increases, while the fraction of particles larger than 3.15 nm decreases. In other words, with increasing temperature, ABS emits larger amount of not only NCA sized particles but also particles in SMPS size range that are larger in size. This suggests that there is a smaller amount of over 57 nm particles present. The observation that both the GMD of larger particles increases and the number of NCA simultaneously grows with increasing temperature is broadly consistent with an assumption that the higher temperature causes more nonvolatile vapors to be emitted at the nozzle. These vapors then rapidly form NCA-sized particles, but also contribute to condensation of larger particles, which then grow to larger sizes by this condensation process. The highest fractions of NCA are found for PLA, 34.7 to 40.4 %, and at high temperatures for nGEN, 41.4 to 48.0 %. Moreover, for nGEN and PLA, as the nozzle temperature increases, they emit larger amount of particles smaller in size (lower GMD_{SMPS}), and simultaneously, NCA emissions increase.

In earlier studies, number emissions have been measured for larger size ranges starting from 3-4 nanometers;[35] however, our findings show that a significant fraction of 3D printing number emissions have been previously unquantified.

Due to the high number of nanoclusters present, the aerosols observed during 3D printing seem to be formed by initial cluster formation and nucleation of gaseous low volatility compounds. The formed clusters act as seeds for consequent condensation and coagulation processes finally forming the observed aerosol distribution. Similar hypothesis has been earlier visited by Vance et al.,[17] who suggested that the aerosols might be formed from semivolatile compounds emitted at the nozzle temperatures, which then nucleate and condensate after cooling down to the room temperatures.

Comparison to previously published literature. As a comparison point to the results of this study, we calculated the fraction of NCA concentration to the total concentration (N_{NCA}/N_{tot}) from the data of Mendes et al.,[34] see Table 1, for ABS and PLA

materials printed in different temperatures. The NCA concentration fractions from Mendes et al. range from 65.8 to 99.2 percent, while similar fractions obtained from this study are significantly lower ranging from 9.7 to 46.7 %. This might result from different approach of calculating the total concentration, see the footer of Table 1, or from the fact that Mendes et al. used chamber air exchange rate of 280 h^{-1}, while we used a lower rate of 20 h^{-1}. Actually, having lower air exchange rate would yield to higher concentrations in the chamber due to slower dilution, however, this is not the case, since we observed lower concentrations with lower air exchange rate. This suggests that the NCA emission rates could, in reality, be even higher than presented in this study. This possibility was already discussed in previous sections, as the particle losses in the diluter and the deposition losses in the chamber involve size dependence, which could not be quantified.

As another point, the total emission rates calculated from SMPS data can be compared to those of others, who measured particle emissions in size ranges starting from 2.5-4.5 nm,[34] 10 nm,[12,18] 15 nm[17] and 17 nm[16] in chambers with similar size as used in this study. The SMPS emission rates for ABS are aligned with the literature, although the values vary up to three orders of magnitude between the studies. The rates for PLA are also in the range of literature values, and mostly one to two orders of magnitude lower than those for ABS with the exception of a few data points. The emission rates in literature for PLA with wood or copper additives are more than two orders of magnitude lower than the ones obtained here showing a potential for further studies. Moreover, to the knowledge of authors, the emissions from nGEN polymer have not been studied before and, thus, direct comparison to literature is not possible. However, the literature offers studies[16,18] for other synthetic polymers, such as polyvinyl alcohol (PVA). When compared to nGEN at high temperatures, the order of magnitude of the emissions are similar, whereas for lower temperatures, nGEN has approximately an order of magnitude lower emissions than PVA. Essentially, the high variation between the studies might be explained by different size ranges considered since 3D printing have shown to emit particles that are below the detection limit for the most of

Table 1: Comparison of the average steady-state number concentrations N (cm^{-3}) and emissions rates Q (s^{-1}) of this study to literature values for SMPS, NCA and total size ranges.

Material	$T_N/T_B^{\star}$	GMD^{*}_{SMPS}	N_{SMPS}	Q_{SMPS}	N_{NCA}	Q_{NCA}	$N^{\ddagger}_{tot}$	Q_{tot}	N_{SMPS}/N_{tot}	Q_{SMPS}/Q_{tot}	N_{NCA}/N_{tot}	Q_{NCA}/Q_{tot}
This study												
ABS	250/90	18.3	$3.2{\cdot}10^{3}$	$1.6{\cdot}10^{7}$	$2.2{\cdot}10^{3}$	$9.7{\cdot}10^{6}$	$1.0{\cdot}10^{4}$	$4.7{\cdot}10^{7}$	0.317	0.315	0.213	0.208
ABS	250/90	21.5	$4.1{\cdot}10^{4}$	$1.9{\cdot}10^{8}$	$1.1{\cdot}10^{4}$	$5.5{\cdot}10^{7}$	$3.7{\cdot}10^{4}$	$1.8{\cdot}10^{8}$	1.094	0.983	0.285	0.305
ABS	240/90	13.3	$1.1{\cdot}10^{3}$	$5.4{\cdot}10^{6}$	$1.1{\cdot}10^{3}$	$5.2{\cdot}10^{6}$	$7.1{\cdot}10^{3}$	$3.2{\cdot}10^{7}$	0.160	0.161	0.155	0.164
PLA	210/60	14.7	$5.7{\cdot}10^{2}$	$2.6{\cdot}10^{6}$	$6.4{\cdot}10^{2}$	$2.8{\cdot}10^{6}$	$1.9{\cdot}10^{3}$	$8.2{\cdot}10^{6}$	0.305	0.303	0.344	0.347
PLA	210/60	12.0	$4.0{\cdot}10^{2}$	$1.8{\cdot}10^{6}$	$6.7{\cdot}10^{2}$	$2.9{\cdot}10^{6}$	$1.6{\cdot}10^{3}$	$7.2{\cdot}10^{6}$	0.243	0.235	0.405	0.404
PLA	220/60	9.9	$1.5{\cdot}10^{3}$	$6.8{\cdot}10^{6}$	$2.1{\cdot}10^{3}$	$8.7{\cdot}10^{6}$	$5.7{\cdot}10^{3}$	$2.4{\cdot}10^{7}$	0.263	0.263	0.368	0.360
PLA	220/60	9.1	$1.0{\cdot}10^{3}$	$4.4{\cdot}10^{6}$	$1.8{\cdot}10^{3}$	$7.4{\cdot}10^{6}$	$4.4{\cdot}10^{3}$	$1.9{\cdot}10^{7}$	0.236	0.225	0.405	0.398
nGEN	240/80	9.4	$2.5{\cdot}10^{3}$	$1.2{\cdot}10^{7}$	$4.8{\cdot}10^{3}$	$2.3{\cdot}10^{7}$	$1.2{\cdot}10^{4}$	$5.4{\cdot}10^{7}$	0.212	0.209	0.414	0.415
nGEN	240/80	8.0	$6.4{\cdot}10^{3}$	$3.2{\cdot}10^{7}$	$1.0{\cdot}10^{4}$	$4.8{\cdot}10^{7}$	$2.4{\cdot}10^{4}$	$1.2{\cdot}10^{8}$	0.262	0.261	0.415	0.414
nGEN	220/80	12.2	$1.6{\cdot}10^{3}$	$7.8{\cdot}10^{6}$	$5.9{\cdot}10^{2}$	$2.5{\cdot}10^{6}$	$3.0{\cdot}10^{3}$	$1.3{\cdot}10^{7}$	0.548	0.555	0.196	0.191
nGEN	220/80	14.5	$1.5{\cdot}10^{3}$	$7.1{\cdot}10^{6}$	$3.2{\cdot}10^{2}$	$1.4{\cdot}10^{6}$	$2.5{\cdot}10^{3}$	$1.1{\cdot}10^{7}$	0.620	0.614	0.130	0.132
nGEN	250/80	9.7	$7.3{\cdot}10^{5}$	$3.8{\cdot}10^{9}$	$8.4{\cdot}10^{5}$	$5.3{\cdot}10^{9}$	$2.0{\cdot}10^{6}$	$1.2{\cdot}10^{10}$	0.363	0.293	0.418	0.424
nGEN	250/80	9.7	$7.4{\cdot}10^{5}$	$3.8{\cdot}10^{9}$	$1.1{\cdot}10^{6}$	$7.3{\cdot}10^{9}$	$2.4{\cdot}10^{6}$	$1.5{\cdot}10^{10}$	0.314	0.240	0.467	0.480
PLA+W	220/60	23.1	$8.6{\cdot}10^{4}$	$3.9{\cdot}10^{8}$	$3.6{\cdot}10^{4}$	$1.9{\cdot}10^{8}$	$3.0{\cdot}10^{5}$	$1.6{\cdot}10^{9}$	0.288	0.235	0.121	0.119
PLA+W	220/60	21.7	$1.0{\cdot}10^{5}$	$4.9{\cdot}10^{8}$	$3.0{\cdot}10^{4}$	$1.6{\cdot}10^{8}$	$3.1{\cdot}10^{5}$	$1.7{\cdot}10^{9}$	0.327	0.279	0.097	0.093
PLA+W	210/60	23.8	$8.5{\cdot}10^{4}$	$4.1{\cdot}10^{8}$	$3.5{\cdot}10^{4}$	$2.2{\cdot}10^{8}$	$2.7{\cdot}10^{5}$	$1.5{\cdot}10^{9}$	0.311	0.264	0.127	0.145
nGEN	250/80	11.3	$2.7{\cdot}10^{4}$	$1.4{\cdot}10^{8}$	$4.4{\cdot}10^{4}$	$2.4{\cdot}10^{8}$	$1.1{\cdot}10^{5}$	$5.4{\cdot}10^{8}$	0.250	0.240	0.416	0.434
ABS	250/90	17.5	$1.9{\cdot}10^{4}$	$9.2{\cdot}10^{7}$	$1.7{\cdot}10^{4}$	$8.6{\cdot}10^{7}$	$6.7{\cdot}10^{4}$	$3.3{\cdot}10^{8}$	0.282	0.267	0.260	0.263
ABS	250/90	20.8	$1.4{\cdot}10^{4}$	$7.1{\cdot}10^{7}$	$1.1{\cdot}10^{4}$	$5.4{\cdot}10^{7}$	$5.5{\cdot}10^{4}$	$2.7{\cdot}10^{8}$	0.255	0.257	0.197	0.204
ABS	250/90	20.8	$1.8{\cdot}10^{4}$	$8.5{\cdot}10^{7}$	$1.3{\cdot}10^{4}$	$6.5{\cdot}10^{7}$	$5.7{\cdot}10^{4}$	$2.7{\cdot}10^{8}$	0.309	0.295	0.234	0.238
PLA+Cu	220/60	9.2	$1.9{\cdot}10^{5}$	$9.1{\cdot}10^{8}$	$1.4{\cdot}10^{5}$	$6.3{\cdot}10^{8}$	$5.9{\cdot}10^{5}$	$2.8{\cdot}10^{9}$	0.326	0.308	0.231	0.225
PLA+Cu	220/60	10.4	$1.4{\cdot}10^{5}$	$6.8{\cdot}10^{8}$	$1.0{\cdot}10^{5}$	$4.6{\cdot}10^{8}$	$4.5{\cdot}10^{5}$	$2.1{\cdot}10^{9}$	0.317	0.300	0.222	0.216
Literature												
ABS-1a [34]	230	$8.8^{\dagger}$	$2.6{\cdot}10^{4}$	$3.7{\cdot}10^{8}$	$1.2{\cdot}10^{6}$		$1.3{\cdot}10^{6}$		0.021		0.979	
ABS-1b [34]	230	$15.5^{\dagger}$	$4.4{\cdot}10^{4}$	$6.2{\cdot}10^{9}$	$2.0{\cdot}10^{6}$		$2.1{\cdot}10^{6}$		0.021		0.979	
ABS-2 [34]	230	$7.9^{\dagger}$	$9.8{\cdot}10^{4}$	$1.4{\cdot}10^{9}$	$2.1{\cdot}10^{6}$		$2.2{\cdot}10^{6}$		0.045		0.955	
ABS-3 [34]	238	$12.8^{\dagger}$	$2.8{\cdot}10^{6}$	$3.9{\cdot}10^{10}$	$5.4{\cdot}10^{6}$		$8.2{\cdot}10^{6}$		0.342		0.658	
ABS-4 [34]	250	$10.5^{\dagger}$	$1.5{\cdot}10^{6}$	$2.2{\cdot}10^{10}$	$4.3{\cdot}10^{6}$		$5.8{\cdot}10^{6}$		0.260		0.740	
PLA-1 [34]	200	-	$7.4{\cdot}10^{2}$	$1.0{\cdot}10^{7}$	$8.9{\cdot}10^{4}$		$8.9{\cdot}10^{4}$		0.008		0.992	
PLA-2 [34]	230	$7.9^{\dagger}$	$3.7{\cdot}10^{5}$	$5.2{\cdot}10^{9}$	$1.4{\cdot}10^{6}$		$1.8{\cdot}10^{6}$		0.205		0.795	

*The nozzle T_N and bed temperatures T_B (°C). *Geometric mean particle count diameter (GMD, nm) for the SMPS data in measurement range of 4.0 - 57.3 nm. †SMPS measurement range from 4.45 to 140.7 nm and chamber air exchange rate of 280 h^{-1}. ‡For the data in this study, N_{tot} is the total concentration from the PSM data (N_{NCA} + $N_{>3nm}$), while for Mendes et al. data,[34] N_{tot} is calculated as N_{NCA} + N_{SMPS}.

the previously applied methodologies.[35]

In a wider context, it is to be noted that different measurement approaches could play a role as well. This has been previously discussed by Pelley et al.[52] and Byrley et al.,[35] who have also pointed out the need for standard measurement method for characterization of 3D printer emissions. In fact, an ANSI/CAN/UL standard has been published.[53] However, the testing protocol suggested therein does not include the size range under 10 nm, thus missing the NCA size range. Furthermore, the Danish EPA presented a risk assessment guidance for 3D printers[54] based on studies[7,12,15,22] that measured the size range starting from 7 or 10 nm. We suggest that risk assessment on 3D printers and the standardized measurement schemes also include the NCA size range as they add a significant contribution to the nanoparticle population.

Comparison of the exposure potential in two distinct environments. The emission rates were used to model consequent dispersion and concentration in two indoor environments. This shows an example of translating the emission rate into an exposure concentration by using information on the room size and ventilation rate. We get an estimate of the concentration addition to the room and thus, of how the printing affects indoor air quality.

Figure 5 presents the concentration addition as a function of distance from the printer for a) high and b) normally ventilated environments in three different emission situations: high ($9.5{\cdot}10^9$ s^{-1}, nGEN at 250°C), medium ($2.2{\cdot}10^8$ s^{-1}, ABS at 250°C) and low ($7.7{\cdot}10^6$ s^{-1}, PLA at 210°C). The concentrations are significantly higher near the printer at 0.35 m, representing working right next to the printer, compared to situations in which the user observes the printing from a distance to the source (1 or 2 m).

To put the results into perspective, the modeled concentrations are compared to existing 8 h/day occupational exposure limit (OEL)[55] recommendations for biopersistent engineered nanoparticles (ENPs), as no limit values are available for incidental nanoscale particle emissions. The OELs for ENPs range from 20 000 cm^{-3} for particles with density over 6000

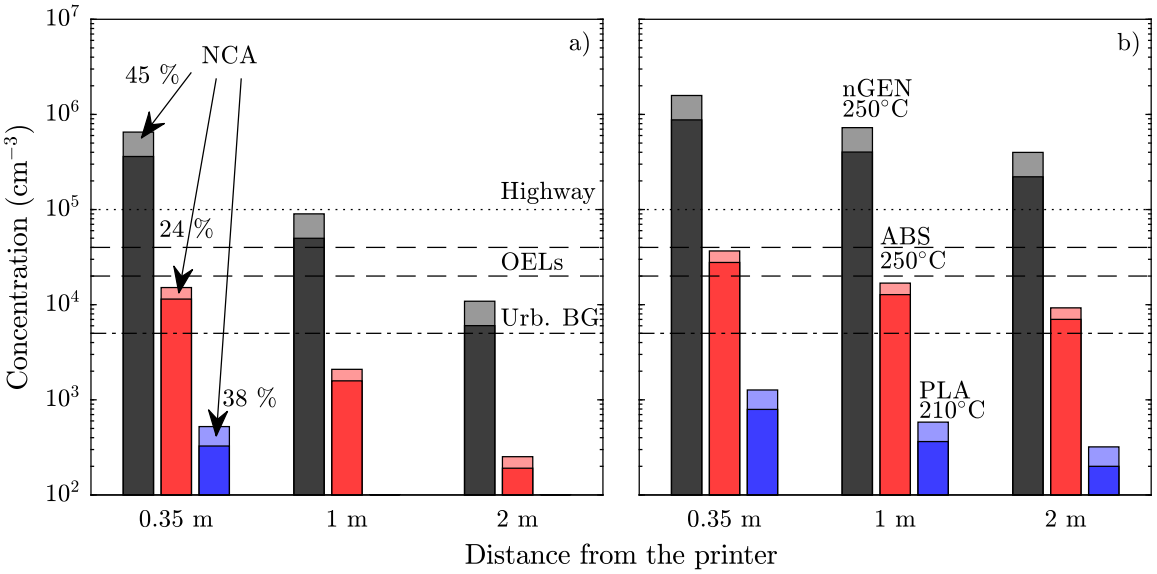

Figure 5: The modeled NCA and total concentrations a) in a well-ventilated (18 h^{-1}) laboratory room with dimensions of 9 m x 6 m x 3 m and b) in a room representing home or small office space, dim. 4 m x 4 m x 2.5 m, with a normal ventilation rate of 0.5 h^{-1}. The assessment was done for three emission situations: high (nGEN, black), medium (ABS, red) and low (PLA, blue). The arrows indicate the percentage of NCA from the total concentration. The horizontal lines from top to bottom represent the average concentration on highways,[36] the range of existing occupational exposure limits (OELs) for biopersistent engineered nanoparticles[55] and urban background concentrations.[36]

kg/m^3 to 40 000 cm^{-3} for particles with density under 6000 kg/m^3. As the densities of plastics, such as ABS and PLA, vary from 900 to 1500 kg/m^3, we use the latter OEL as a comparison point. However, it is not known whether this value serves as a protective limit for 3D printer emissions. In the high ventilated laboratory room (Fig. 5a), in the high emission case, the concentrations closer than 1 meter are clearly above the OEL limit due to the NCA addition, while the concentration at 2 m stands under the OEL. The medium and low emission cases result mainly in lower than OEL concentrations, although, in very close proximity $<$ 0.35 m, the NCA addition lifts the total concentration above the urban background.

In comparison, the normally ventilated home, school or office environment (Fig. 5b) shows similar tendency with approximately 2.4, 8.1 and 36.7 times higher concentrations, respectively, depending on the distance. Consequently, the concentrations in the medium

emission case exceed urban background concentrations barely staying under the OEL near the printer due to the NCA addition. On the contrary, in the high emission case, the concentrations increase to extreme figures even far away from the printer.

All things considered, laboratories and production facilities with high ventilation that are designed to host industrial processes seem to dilute the aerosol enough to reach low enough exposure concentrations in medium and low emission cases. However, in a home, school or office with relatively low ventilation designed to keep only the CO_2 level low enough, the user may get a high dose when the printer is run long and continuously in the presence of the user. Therefore, the users should stay away from the printer while it is running due to high exposure potential. Note that this analysis considers only the case of one printer; operating multiple printers in the same room would increase concentrations over the OELs also further away from the source.[1]

Some emission prevention techniques are available, such as local exhaust ventilation, sealed framing and filtering of the exhaust air from the printer, that can overcome these issues if used properly. However, in the light of this study, the methods used to limit the emission should be designed to filter the smallest NCA particles as well.

Acknowledgement

We would like to thank Dr. Luis Mendes and Prof. Katrianne Lehtipalo at University of Helsinki and Dr. Anna-Kaisa Viitanen at Finnish Institute of Occupational Health for sharing the PSM number concentration data presented in Fig. 2 of Mendes et al.[34] as well as the raw concentration data. This allowed calculation of average NCA number concentrations and NCA fractions as a comparison to the results presented in this paper. The authors thank Airmodus Ltd for the nCNC A11 instrumentation employed in this study and for the help provided on the analysis of the PSM calibration data (Elina Miettinen and Dr. Joonas Vanhanen). We thank Prof. Jorma Keskinen for useful discussions. The authors acknowledge

Tampere University Graduate School as well as the Maj and Tor Nessling Foundation (Grant no. 201700520) for financial support.

Supporting Information Available

This information is available free of charge via the Internet at http://pubs.acs.org.

- Supporting Information.pdf: Properties of the printer and the printed object, list of printing events including successful and failed prints, CPC comparison, PSM calibration data, the source code used for indoor dispersion modeling and figures on the time evolution of the particle number concentrations and size distributions during the printing process.

References

(1) Bharti, N.; Singh, S. Three-dimensional (3D) printers in libraries: Perspective and preliminary safety analysis. *Journal of chemical education* **2017**, *94*, 879–885.

(2) Wojtyła, S.; Klama, P.; Baran, T. Is 3D printing safe? Analysis of the thermal treatment of thermoplastics: ABS, PLA, PET, and nylon. *Journal of occupational and environmental hygiene* **2017**, *14*, D80–D85.

(3) Chan, F.; House, R.; Kudla, I.; Lipszyc, J.; Rajaram, N.; Tarlo, S. Health survey of employees regularly using 3D printers. *Occupational Medicine* **2018**, *68*, 211–214.

(4) Gümperlein, I.; Fischer, E.; Dietrich-Gümperlein, G.; Karrasch, S.; Nowak, D.; Jörres, R. A.; Schierl, R. Acute health effects of desktop 3D printing (fused deposition modeling) using acrylonitrile butadiene styrene and polylactic acid materials: An experimental exposure study in human volunteers. *Indoor Air* **2018**, *28*, 611–623.

(5) Stefaniak, A.; LeBouf, R.; Duling, M.; Yi, J.; Abukabda, A.; McBride, C.; Nurkiewicz, T. Inhalation exposure to three-dimensional printer emissions stimulates acute hypertension and microvascular dysfunction. *Toxicology and applied pharmacology* **2017**, *335*, 1–5.

(6) de Almeida Monteiro Melo Ferraz, M.; Henning, H. H.; Ferreira da Costa, P.; Malda, J.; Le Gac, S.; Bray, F.; van Duursen, M. B.; Brouwers, J. F.; van de Lest, C. H.; Bertijn, I.; Kraneburg, L.; Vos, P. L. A. M.; Stout, T. A. E.; Gadella, B. M. Potential Health and Environmental Risks of Three-Dimensional Engineered Polymers. *Environmental science & technology letters* **2018**, *5*, 80–85.

(7) Stephens, B.; Azimi, P.; El Orch, Z.; Ramos, T. Ultrafine particle emissions from desktop 3D printers. *Atmospheric Environment* **2013**, *79*, 334–339.

(8) Farcas, M. T.; Stefaniak, A. B.; Knepp, A. K.; Bowers, L.; Mandler, W. K.; Kashon, M.; Jackson, S. R.; Stueckle, T. A.; Sisler, J. D.; Friend, S. A.; Qi, C.; Hammond, D. R.; Thomas, T. A.; Matheson, J.; Castranova, V.; Qian, Y. Acrylonitrile butadiene styrene (ABS) and polycarbonate (PC) filaments three-dimensional (3-D) printer emissions-induced cell toxicity. *Toxicology Letters* **2019**, *317*, 1–12.

(9) Zhang, Q.; Pardo, M.; Rudich, Y.; Kaplan-Ashiri, I.; Wong, J. P. S.; Davis, A. Y.; Black, M. S.; Weber, R. J. Chemical Composition and Toxicity of Particles Emitted from a Consumer-level 3D Printer using Various Materials. *Environmental Science & Technology* **2019**, *53*, 12054–12061.

(10) Yang, W.; Peters, J. I.; Williams III, R. O. Inhaled nanoparticles-a current review. *International Journal of Pharmaceutics* **2008**, *356*, 239–247.

(11) Oberdörster, G.; Oberdörster, E.; Oberdörster, J. Nanotoxicology: an emerging discipline evolving from studies of ultrafine particles. *Environmental health perspectives* **2005**, *113*, 823–839.

(12) Kim, Y.; Yoon, C.; Ham, S.; Park, J.; Kim, S.; Kwon, O.; Tsai, P.-J. Emissions of nanoparticles and gaseous material from 3D printer operation. *Environmental science & technology* **2015**, *49*, 12044–12053.

(13) Afshar-Mohajer, N.; Wu, C.-Y.; Ladun, T.; Rajon, D. A.; Huang, Y. Characterization of particulate matters and total VOC emissions from a binder jetting 3D printer. *Building and Environment* **2015**, *93*, 293–301.

(14) Mellin, P.; Jönsson, C.; Åkermo, M.; Fernberg, P.; Nordenberg, E.; Brodin, H.; Strondl, A. Nano-sized by-products from metal 3D printing, composite manufacturing and fabric production. *Journal of cleaner production* **2016**, *139*, 1224–1233.

(15) Azimi, P.; Zhao, D.; Pouzet, C.; Crain, N. E.; Stephens, B. Emissions of ultrafine particles and volatile organic compounds from commercially available desktop three-dimensional printers with multiple filaments. *Environmental science & technology* **2016**, *50*, 1260–1268.

(16) Floyd, E. L.; Wang, J.; Regens, J. L. Fume emissions from a low-cost 3-D printer with various filaments. *Journal of occupational and environmental hygiene* **2017**, *14*, 523–533.

(17) Vance, M. E.; Pegues, V.; Van Montfrans, S.; Leng, W.; Marr, L. C. Aerosol Emissions from Fuse-Deposition Modeling 3D Printers in a Chamber and in Real Indoor Environments. *Environmental Science & Technology* **2017**, *51*, 9516–9523.

(18) Kwon, O.; Yoon, C.; Ham, S.; Park, J.; Lee, J.; Yoo, D.; Kim, Y. Characterization and control of nanoparticle emission during 3D printing. *Environmental science & technology* **2017**, *51*, 10357–10368.

(19) Rao, C.; Gu, F.; Zhao, P.; Sharmin, N.; Gu, H.; Fu, J. Capturing PM2. 5 emissions from 3D printing via nanofiber-based air filter. *Scientific reports* **2017**, *7*, 10366.

(20) Stabile, L.; Scungio, M.; Buonanno, G.; Arpino, F.; Ficco, G. Airborne particle emission of a commercial 3D printer: The effect of filament material and printing temperature. *Indoor Air* **2017**, *27*, 398–408.

(21) Stefaniak, A. B.; LeBouf, R. F.; Yi, J.; Ham, J.; Nurkewicz, T.; Schwegler-Berry, D. E.; Chen, B. T.; Wells, J. R.; Duling, M. G.; Lawrence, R. B.; Martin Jr., S. B.; Johnson, A. R.; Virji, M. A. Characterization of chemical contaminants generated by a desktop fused deposition modeling 3-dimensional Printer. *Journal of occupational and environmental hygiene* **2017**, *14*, 540–550.

(22) Steinle, P. Characterization of emissions from a desktop 3D printer and indoor air measurements in office settings. *Journal of occupational and environmental hygiene* **2016**, *13*, 121–132.

(23) Yi, J.; LeBouf, R. F.; Duling, M. G.; Nurkiewicz, T.; Chen, B. T.; Schwegler-Berry, D.; Virji, M. A.; Stefaniak, A. B. Emission of particulate matter from a desktop three-dimensional (3D) printer. *Journal of Toxicology and Environmental Health, Part A* **2016**, *79*, 453–465.

(24) Zhang, Q.; Wong, J. P.; Davis, A. Y.; Black, M. S.; Weber, R. J. Characterization of particle emissions from consumer fused deposition modeling 3D printers. *Aerosol Science and Technology* **2017**, *51*, 1275–1286.

(25) Zhou, Y.; Kong, X.; Chen, A.; Cao, S. Investigation of Ultrafine Particle Emissions of Desktop 3D Printers in the Clean Room. *Procedia Engineering* **2015**, *121*, 506–512.

(26) Zontek, T. L.; Ogle, B. R.; Jankovic, J. T.; Hollenbeck, S. M. An exposure assessment of desktop 3D printing. *Journal of Chemical Health and Safety* **2017**, *24*, 15–25.

(27) Du Preez, S.; Johnson, A.; LeBouf, R. F.; Linde, S. J.; Stefaniak, A. B.; Du Plessis, J. Exposures during industrial 3-D printing and post-processing tasks. *Rapid Prototyping Journal* **2018**, *24*, 865–871.

(28) Stefaniak, A. B.; Bowers, L. N.; Knepp, A. K.; Virji, M. A.; Birch, E. M.; Ham, J. E.; Wells, J. R.; Qi, C.; Schwegler-Berry, D.; Friend, S.; Johnson, A. R.; Martin Jr, S. B.; Qian, Y.; LeBouf, R. F.; Birch, Q.; Hammond, D. Three-dimensional printing with nano-enabled filaments releases polymer particles containing carbon nanotubes into air. *Indoor Air* **2018**, *28*, 840–851.

(29) Simon, T. R.; Lee, W. J.; Spurgeon, B. E.; Boor, B. E.; Zhao, F. An Experimental Study on the Energy Consumption and Emission Profile of Fused Deposition Modeling Process. *Procedia Manufacturing* **2018**, *26*, 920–928.

(30) Cheng, Y.-L.; Zhang, L.-C.; Chen, F.; Tseng, Y.-H. Particle Emissions of Material-Extrusion-Type Desktop 3D Printing: the Effects of Infill. *International Journal of Precision Engineering and Manufacturing-Green Technology* **2018**, *5*, 487–497.

(31) Stefaniak, A.; Johnson, A.; du Preez, S.; Hammond, D.; Wells, J.; Ham, J.; LeBouf, R.; Menchaca, K.; Martin, S.; Duling, M.; Bowers, L.; Knepp, A.; Su, F.; de Beer, D.; du Plessis, J. Evaluation of emissions and exposures at workplaces using desktop 3-dimensional printers. *Journal of Chemical Health and Safety* **2019**, *26*, 19–30.

(32) Stefaniak, A.; Johnson, A.; du Preez, S.; Hammond, D.; Wells, J.; Ham, J.; LeBouf, R.; Martin, S.; Duling, M.; Bowers, L.; Knepp, A.; de Beer, D.; du Plessis, J. Insights Into Emissions and Exposures From Use of Industrial-Scale Additive Manufacturing Machines. *Safety and Health at Work* **2019**, *10*, 229–236.

(33) Deng, Y.; Cao, S.-J.; Chen, A.; Guo, Y. The impact of manufacturing parameters on submicron particle emissions from a desktop 3D printer in the perspective of emission reduction. *Building and Environment* **2016**, *104*, 311–319.

(34) Mendes, L.; Kangas, A.; Kukko, K.; Mølgaard, B.; Säämänen, A.; Kanerva, T.; Flores Ituarte, I.; Huhtiniemi, M.; Stockmann-Juvala, H.; Partanen, J.; Hämeri, K.; Eleft-

heriadis, K.; Viitanen, A.-K. Characterization of emissions from a desktop 3D printer. *Journal of Industrial Ecology* **2017**, *21*, S94–S106.

(35) Byrley, P.; George, B. J.; Boyes, W. K.; Rogers, K. Particle emissions from fused deposition modeling 3D printers: Evaluation and meta-analysis. *Science of The Total Environment* **2019**, *655*, 395 – 407.

(36) Rönkkö, T.; Kuuluvainen, H.; Karjalainen, P.; Keskinen, J.; Hillamo, R.; Niemi, J. V.; Pirjola, L.; Timonen, H. J.; Saarikoski, S.; Saukko, E.; Järvinen, A.; Silvennoinen, H.; Rostedt, A.; Olin, M.; Yli-Ojanperä, J.; Nousiainen, P.; Kousa, A.; Maso, M. D. Traffic is a major source of atmospheric nanocluster aerosol. *Proceedings of the National Academy of Sciences* **2017**, *114*, 7549–7554.

(37) Maher, B. A.; Ahmed, I. A. M.; Karloukovski, V.; MacLaren, D. A.; Foulds, P. G.; Allsop, D.; Mann, D. M. A.; Torres-Jardón, R.; Calderon-Garciduenas, L. Magnetite pollution nanoparticles in the human brain. *Proceedings of the National Academy of Sciences* **2016**, *113*, 10797–10801.

(38) Hawkins, S. J.; Crompton, L. A.; Sood, A.; Saunders, M.; Boyle, N. T.; Buckley, A.; Minogue, A. M.; McComish, S. F.; Jiménez-Moreno, N.; Cordero-Llana, O.; Stathakos, P.; Gilmore, C. E.; Kelly, S.; Lane, J. D.; Case, C. P.; Caldwell, M. A. Nanoparticle-induced neuronal toxicity across placental barriers is mediated by autophagy and dependent on astrocytes. *Nature nanotechnology* **2018**, *13*, 427–433.

(39) Ahonen, L.; Kangasluoma, J.; Lammi, J.; Lehtipalo, K.; Hämeri, K.; Petäjä, T.; Kulmala, M. First measurements of the number size distribution of 1–2 nm aerosol particles released from manufacturing processes in a cleanroom environment. *Aerosol Science and Technology* **2017**, *51*, 685–693.

(40) Nosko, O.; Vanhanen, J.; Olofsson, U. Emission of 1.3-10 nm airborne particles from brake materials. *Aerosol Science and Technology* **2017**, *51*, 91–96.

(41) Järvinen, A.; Timonen, H.; Karjalainen, P.; Bloss, M.; Simonen, P.; Saarikoski, S.; Kuuluvainen, H.; Kalliokoski, J.; Dal Maso, M.; Niemi, J. V.; ; Keskinen, J.; Rönkkö, T. Particle emissions of Euro VI, EEV and retrofitted EEV city buses in real traffic. *Environmental Pollution* **2019**, *250*, 708–716.

(42) Hietikko, R.; Kuuluvainen, H.; Harrison, R. M.; Portin, H.; Timonen, H.; Niemi, J. V.; Rönkkö, T. Diurnal variation of nanocluster aerosol concentrations and emission factors in a street canyon. *Atmospheric environment* **2018**, *189*, 98–106.

(43) Kangasniemi, O.; Kuuluvainen, H.; Heikkilä, J.; Pirjola, L.; Niemi, J. V.; Timonen, H.; Saarikoski, S.; Rönkkö, T.; Dal Maso, M. Dispersion of a Traffic Related Nanocluster Aerosol Near a Major Road. *Atmosphere* **2019**, *10*, 309.

(44) Kulmala, M.; Petäjä, T.; Nieminen, T.; Sipilä, M.; Manninen, H. E.; Lehtipalo, K.; Dal Maso, M.; Aalto, P. P.; Junninen, H.; Paasonen, P.; Riipinen, I.; Lehtinen, K. E. J.; Laaksonen, A.; Kerminen, V.-M. Measurement of the nucleation of atmospheric aerosol particles. *Nature protocols* **2012**, *7*, 1651–1667.

(45) Kulmala, M.; Kontkanen, J.; Junninen, H.; Lehtipalo, K.; Manninen, H. E.; Nieminen, T.; Petäjä, T.; Sipilä, M.; Schobesberger, S.; Rantala, P.; Franchin, A.; Jokinen, T.; Järvinen, E.; Äijälä, M.; Kangasluoma, J.; Hakala, J.; Aalto, P. P.; Paasonen, P.; Mikkilä, J.; Vanhanen, J.; Aalto, J.; Hakola, H.; Makkonen, U.; Ruuskanen, T.; Mauldin, R. L.; Duplissy, J.; Vehkamäki, H.; Bäck, J.; Kortelainen, A.; Riipinen, I.; Kurtén, T.; Johnston, M. V.; Smith, J. N.; Ehn, M.; Mentel, T. F.; Lehtinen, K. E. J.; Laaksonen, A.; Kerminen, V.-M.; Worsnop, D. R. Direct observations of atmospheric aerosol nucleation. *Science* **2013**, *339*, 943–946.

(46) Kontkanen, J.; Lehtipalo, K.; Ahonen, L.; Kangasluoma, J.; Manninen, H. E.; Hakala, J.; Rose, C.; Sellegri, K.; Xiao, S.; Wang, L.; Qi, X.; Nie, W.; Ding, A.; Yu, H.; Lee, S.; Kerminen, V.-M.; Petäjä, T.; Kulmala, M. Measurements of sub-3 nm

particles using a particle size magnifier in different environments: from clean mountain top to polluted megacities. *Atmospheric Chemistry and Physics* **2017**, *17*, 2163–2187.

(47) Biswas, P.; Wang, Y.; Attoui, M. Sub-2nm particle measurement in high-temperature aerosol reactors: a review. *Current Opinion in Chemical Engineering* **2018**, *21*, 60–66.

(48) Kangasluoma, J.; Kuang, C.; Wimmer, D.; Rissanen, M.; Lehtipalo, K.; Ehn, M.; Worsnop, D.; Wang, J.; Kulmala, M.; Petäjä, T. Sub-3 nm particle size and composition dependent response of a nano-CPC battery. *Atmospheric Measurement Techniques* **2014**, *7*, 689–700.

(49) Kulkarni, P.; Baron, P. A.; Willeke, K. *Aerosol measurement: principles, techniques, and applications*; John Wiley & Sons, 2011.

(50) Cooper, D. W.; Horowitz, M. Exposures from Indoor Powder Releases: Models and Experiments. *American Industrial Hygiene Association Journal* **1986**, *47*, 214–218.

(51) Drivas, P. J.; Valberg, P. A.; Murphy, B. L.; Wilson, R. Modeling indoor air exposure from short-term point source releases. *Indoor Air* **1996**, *6*, 271–277.

(52) Pelley, J. Safety Standards Aim to Rein in 3-D Printer Emissions. *ACS Central Science* **2018**, *4*, 134–136.

(53) ANSI/CAN/UL Standard Method for Testing and Assessing Particle and Chemical Emissions from 3D Printers. *UL Environment Standard 2904, Underwriters Laboratories Inc., USA* **2019**, *Edition 1*, Edition Date: January 31, 2019.

(54) Jacobsen, E.; Nielsen, I. B.; Schjøth-Eskesen, J.; Fischer, C. H.; Larsen, P. B.; Andersen, D. N.; Eds., Risk Assessment of 3D Printers and 3D Printed Products. *Survey of chemical substances in consumer products, The Danish Environmental Protection Agency, Copenhagen, Denmark* **2017**, *161*, 1–90.

(55) Schulte, P. A.; Murashov, V.; Zumwalde, R.; Kuempel, E. D.; Geraci, C. L. Occupational exposure limits for nanomaterials: state of the art. *Journal of Nanoparticle Research* **2010**, *12*, 1971–1987.

Graphical TOC Entry